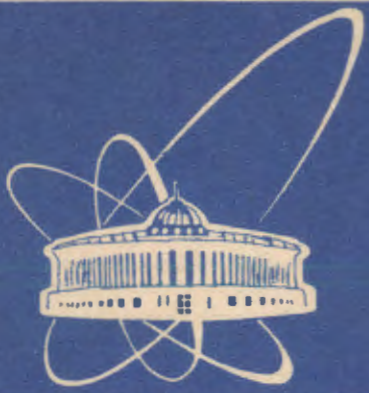

СООБЩЕНИЯ
ОБЪЕДИНЕННОГО
ИНСТИТУТА
ЯДЕРНЫХ
ИССЛЕДОВАНИЙ

Дубна

E3-95-445

Yu.M.Gledenov, G.Khuukhenkhuu, M.V.Sedysheva,
Bao Shanglian[1], Tang Guoyou[1], Cao Wentian[1], Qu Decheng[1],
Chen Zemin[2], Chen Yingtang[2], Qi Huiquan[2]

INVESTIGATION OF THE FAST NEUTRON INDUCED (n,α) REACTION (Experimental Techniques)

[1]Peking University, Beijing, P.R. China
[2]Tsinghua University, Beijing, P.R. China

1995

1. INTRODUCTION

Investigation of charged particle emission reactions induced by fast neutrons is of considerable interest for both nuclear energy applications and the understanding of basic nuclear problems. For example, these reactions lead to a buildup of residual radioactivity and radiation damage due to hydrogen and helium gas production in the structural materials of fission and fusion reactors [1]. On the other hand, systematic study of such reactions depending on neutron energy allows the contributions of compound, pre-equilibrium and direct processes to the studied reactions to be determined [2]. However, nuclear data compilations [3,4] show that at energies between 3 and 10 MeV, where the threshold of many of the charged particle emission reactions lie, the experimental data base is rather sparse and there are significant discrepancies between the available results of various authors. In addition, in most cases, previous measurements of these reactions in this energy range were made using activation techniques. This method, though easier in practice, is feasible only in certain cases where the residual nuclei reached by charged particle emission are unstable. Also, such measurements do not allow the energy spectra and angular distributions to be obtained for the emitted charged particles. Over the years, numerous charged particle detectors have been developed and successfully used in the neutron energy range of ~10-14 MeV [5-8]. Nevertheless, at energies E_n<10 MeV these methods, due to their small solid angle-efficiency and low counting rate, were rarely used.

Therefore, in 1990 we started the development and testing of a gridded, gas filled twin ionization chamber to study the charged particle emission reactions induced by neutrons of several MeV [9]. Such measurements are difficult because of low cross sections and require the use of a high flux neutron source and a low background - high luminosity charged particle spectrometer.

In this paper we describe experimental techniques based on the gridded ionization chambers which were specially developed, tested and used for the investigation of fast neutron induced charged particle emission reactions. Also, as examples, some of our results obtained on the medium mass nuclei are given [10-13].

It should be noted that in recent years Baba et al. [14] and Goverdovski et al. [15] have also been using a gridded ionization chamber for studying fast neutron induced reactions.

2. NEUTRON SOURCE AND FLUX

Nearly monoenergetic neutrons of several MeV were produced via the $D(d,n)^3He$ reaction using a water cooled thin solid Ti-D target backed by copper foil 1 mm thick. Experiments were carried out at the 4.5 MeV Van de Graaf accelerator at the Institute of Heavy Ion Physics, Peking University, Beijing, P.R. China. The spread and mean energy of incident neutrons on a flat circular sample at a given distance from the Ti-D target were calculated using the kinematic formulae [16,17]. The neutron energy spread for all measurements was ΔE_n<300 keV. A neutron beam collimator was not used because the neutron flux on the isotope-sample for almost a point source rapidly decreases with increasing distance from the neutron source. In addition, collimation can lead to contamination of the direct neutron beam by scattered and moderated neutrons. Neutron flux was determined with the help of a previously calibrated BF_3 long counter and a low mass 0.2 mm thick brass fission chamber with enriched (99.997%) ^{238}U. The ^{238}U target and the studied isotope-sample had the same neutron beam solid angle during the measurements. In most cases of our measurements the ^{238}U fission chamber, BF_3 long counter and a gridded ionization chamber which was used to detect charged particles, were placed at zero degrees with respect to the direction of the neutron beam.

3. THE CHARGED PARTICLE DETECTOR

Charged particles emitted in the fast neutron induced reactions were detected using a parallel-plate, grid-type twin ionization chamber with a common cathode, which made a good showing in our measurements with slow neutrons [18]. For our investigation we made two ionization chambers. The choice of which one to use depended on measurement conditions. In order to detect alpha particles of energies up to E_α~15 MeV, a so called low pressure ionization chamber (LPIC) was made that can operate at gas pressures of P<2 atm. For more energetic particles a so called high pressure ionization chamber (HPIC) was constructed which can stand gas pressures up to 5 atm which is high enough to stop ~25 MeV alpha particles and ~7 MeV protons in the working volume. Both ionization chambers were made at the Frank Laboratory of Neutron Physics, JINR, Dubna, Russia. The main advantages of gas filled, gridded ionization chambers are the close to 100% (in 2π geometry) charged particle detection efficiency and a low sensitivity to gamma rays. Such detectors are not damaged by fast neutrons and can be placed directly in a neutron beam. In addition, the gridded ionization chamber allows energy and angular distributions to be obtained as well as the identification of secondary charged particles.

3.1 DESIGN AND CONSTRUCTION OF THE IONIZATION CHAMBERS

A. THE LOW PRESSURE IONIZATION CHAMBER

Schematic views of the LPIC and its inner construction are shown in Figs. 1 and 2, respectively. This twin ionization chamber has, as mentioned above, the common cathode made of thin aluminium or tungsten foil on which the isotope-sample was evaporated in vacuum. Thus, the first section of the twin ionization chamber contains the isotope-sample. At the same time, the second section is empty and is used for background measurements. The anode plates are 0.2 mm thick aluminium foils. The grids consist of parallel gold-coated tungsten wires 0.1 mm in diameter spaced 2 mm apart. The grid wires were soldered to a 2 mm thick rectangular fiberglass frame plated with thin copper foil. The LPIC can work under single or double grid conditions depending on the measurement purpose. In addition, distances between electrodes can be changed within the bounds of the chamber.

Energy calibration of the charged particle spectrometer was performed using uranium or plutonium alpha sources. The alpha sources, with the help of a modified form of the Wilson vacuum-tight sliding seal [19], are moved into the working volume of the chamber for energy calibration and are moved out during the main measurements (see Fig. 1, expanded fragment in the upper part).

The connectors for the high voltage and output signal were bolted to the bottom by means of a brass flange (see Fig. 1, expanded fragment in the lower part). Gas inlet and outlet ports were placed on the top cover of the chamber in which gas pressure is checked by a mano-vacuum-meter.

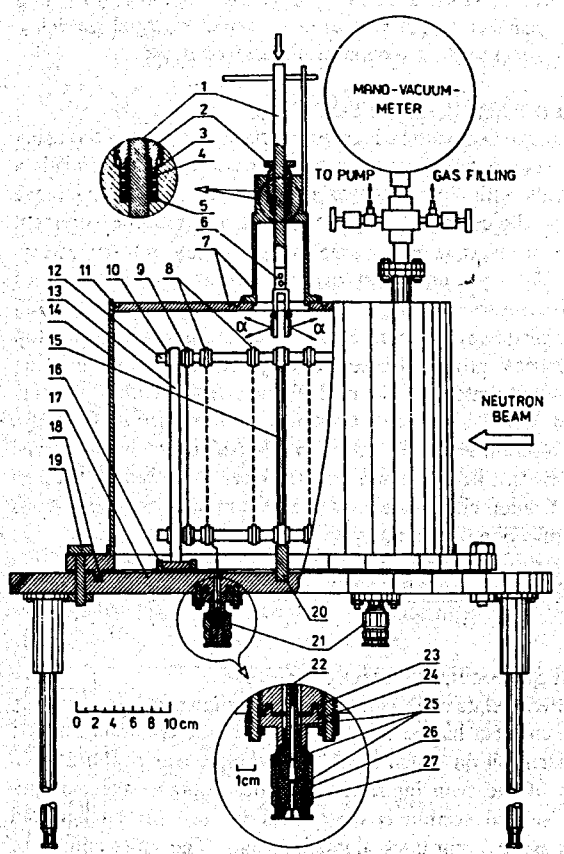

Fig. 1. Schematic view of the low pressure ionization chamber
1 - polished sliding brass rod
2 - nut
3 - metal washer
4 - rubber washer
5 - teflon bushing
6 - teflon insulator
7 - aluminium cover
8 - Frisch grids
9 - anode
10 - teflon nut
11 - welded joint
12 - teflon spindle
13 - aluminium support
14 - aluminium cylinder 3 mm thick
15 - stainless steel plate-holder
16 - teflon insulator
17 - bottom
18 - rubber gasket
19 - bolt
20 - teflon leg
21 - connectors
22 - wire
23 - rubber gasket
24 - brass flange
25 - teflon insulators
26 - brass pivot
27 - cover from the CP-75-54Φ (Russian analogy to BNC) connector plug

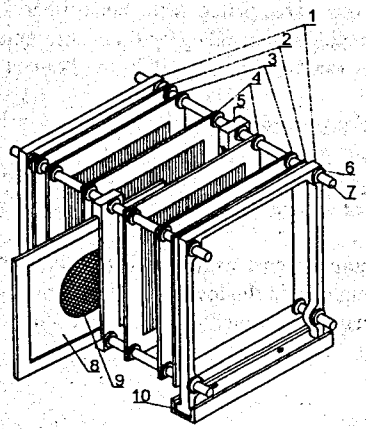

Fig. 2. Inner construction of the LPIC
1 - aluminium supports
2 - anodes
3,4 - Frisch grids
5 - cathode-holder
6 - teflon nut
7 - teflon spindle with thread
8 - cathode
9 - sample
10 - teflon insulator

B. THE HIGH PRESSURE IONIZATION CHAMBER

Schematic views of the HPIC and its inner construction are displayed in Figs. 3 and 4, respectively. The anodes and cathodes are 0.1-0.2 mm thick aluminium foils. The grids are parallel tungsten wires 0.1 mm in diameter spaced 2 mm apart. The grid wires were fastened by electric spot-welding to a stainless steel ring with a 27 cm i.d. and 32 cm o.d. The circular form electrodes are housed in an aluminium tank, having a lid with a 3 mm thick concave aluminium window. The window can stand with gas pressure in the chamber up to 5 atm, minimizes neutron absorption and allows a sample to be brought closer to the neutron source. Alpha sources, in contrast to the LPIC, are moved into the working volume by turning the source-holder with the help of a modified form of the Wilson seal. All connectors are placed on a common brass flange which was bolted to the aluminium cylinder and is opened to make contact with the electrodes. The electrodes are mounted on the lid with three teflon rods. The distances between the electrodes can be changed. The HPIC can also be operated with a single or double grid. The operation of HPIC is very much like that of the LPIC and their sample-holders allow the isotope-sample to be replaced without changing the lay-out of the electrodes.

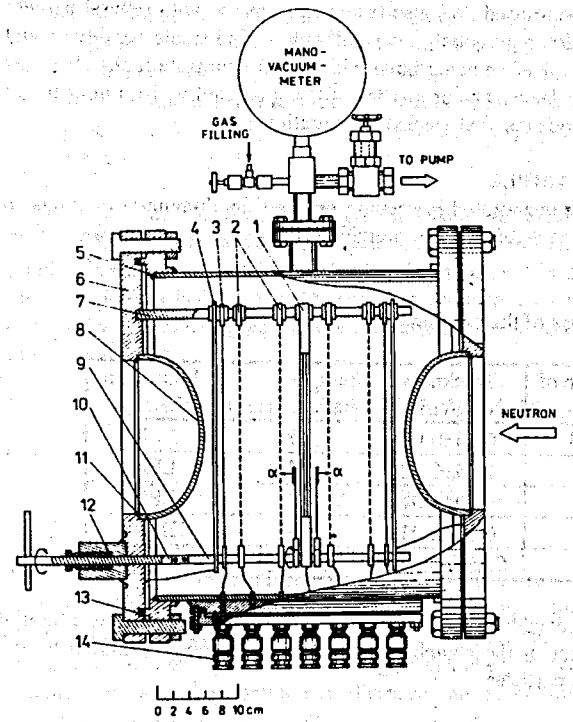

Fig. 3. Schematic view of the high pressure ionization chamber
1 - cathode- holder
2 - grids
3 - anode
4 - aluminium guard ring
5 - aluminium cylinder
6 - lid
7 - teflon support
8 - aluminium window 3 mm thick
9 - teflon rod
10 - polished sliding brass rod
11 - welded joint
12 - modified form of the Wilson seal
13 - rubber gasket
14 - connectors

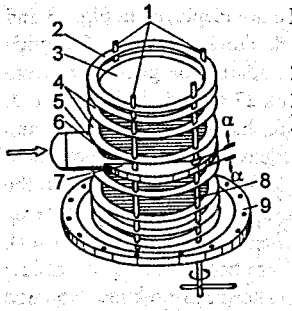

Fig. 4. Inner construction of the HPIC
1 - teflon supports
2 - guard ring
3 - anode
4 - Frisch grids
5 - cathode
6 - sample
7 - aluminium cathode holder
8 - teflon rod
9 - lid

3.2 WORKING GAS

Noble gases mixed with dioxide carbon or methane are usually utilized to fill the ionization chamber [20]. But, in our case, because of background caused by recoil protons, methane was not used though it has high drift velocities. Gas mixtures of Ar+(3-5)%CO_2 or Kr+(1.7-3)%CO_2 were used. We also tested neon mixed with several percent CO_2. But, due to its low breakdown potential, it was difficult to find stable conditions and it was not used in our chambers. Before being filled with gas, the ionization chamber was carefully pumped and tested for leaks. The properties of this gas filled ionization chamber remain unchanged for long periods (several weeks) of operation.

4. ISOTOPE-SAMPLE

The isotope-sample was evaporated in vacuum onto a thin aluminium or tungsten foil. Thickness of the sample was determined by weighing. The basic characteristics of the samples are given in Table 1.

Table 1. The basic characteristics of the samples

Nuclei	Sample	Abundance of isotope (%)	Thickness (mg/cm^2)	Sample diameter (cm)	Ionization chamber
^{40}Ca	CaF_2	Natural	0.86±0.03	5	LPIC
^{58}Ni	metal	99.9	1.05±0.02	4	LPIC
	metal	99.8	0.50±0.01	4	LPIC
^{64}Zn	metal	99.4	0.72±0.03	10	HPIC
	metal	99.4	0.250±0.013	10	HPIC

Sample sizes are determined by the permissible energy spread of neutrons, required neutron fluence and edge effect of the chamber. The sample thickness is limited by the energy loss of emitted charged particles.

5. EXPERIMENTAL SET-UP

A block diagram of the experimental setup as used is shown in Fig. 5. The pulse-height data for the anode and cathode signals were gathered and analysed by a multiparameter data acquisition system based on the IBM PC AT-386 computer and designed at the Institute of Heavy Ion Physics, Peking University [21,22].

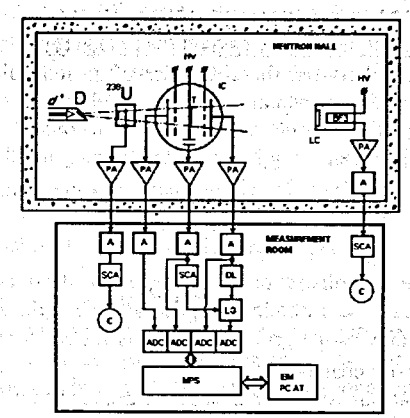

Fig. 5. Block diagram of experimental setup.
d^+ - deuteron ion beam; D - deuterium target; ^{238}U - uranium fission chamber; IC - gridded twin ionization chamber; HV - high voltage supply; LC - long counter; PA - preamplifier; A - main spectroscopy amplifier; SCA - single channel analyzer; C - counter; DL - delay line; LG - linear gate; ADC - analog to digital converter; MPS - multiparameter data acquisition system

6. EXTRACTION OF ENERGY AND ANGLE INFORMATION

The detection principle of gridded ionization chambers has been considered in detail by various authors [14-15,22-25]. In the case of a single grid chamber, the anode and cathode signals for charged particles emitted from a sample placed on the cathode and stopped by the counting gas before reaching the Frisch grid, P_A and P_C, respectively, can be represented as

$$P_A \sim E\left(1+\sigma-\sigma\frac{\overline{X}}{a}\cos\theta\right) \tag{1}$$

and

$$P_C \sim E(1-\frac{\overline{X}}{a}\cos\theta). \tag{2}$$

Here E is the charged particle energy, σ is the grid inefficiency, $\overline{X}$ is the distance from the cathode to the center of gravity of the ionization track , a is the distance between the cathode and the Frisch grid, and θ is the angle between the particle track and the normal of the cathode. Since σ can be less than a few percent, P_A approximately represents the charged particle energy. In our single grid chamber, σ was not worse than 3%. For the double grid case, the common inefficiency can be obtained as [26] $\sigma = \sigma_1 \cdot \sigma_2$, where σ_1 and σ_2 are the shielding inefficiencies of the first and second grids, respectively. In the double grid case the common shielding inefficiency disappears.

Thus, using Eqs. (1) and (2) we can simultaneously obtain both the charged particle energy and the emission angle with the help of the two dimensional spectra of P_A and P_C.

7. TEST MEASUREMENT AND RESULTS

7.1. CHOICE OF WORKING CONDITION FOR THE ELECTRICAL FIELD

The electrical field between the electrodes of an ionization chamber is obtained from the condition of possible maximum velocities for electron drift. In addition, to avoid electron collection by the Frisch grid, the ratio of the electrical field strength between the anode and grid to that between the grid and cathode must fulfill the following condition [24]:

$$\frac{(V_A - V_G)/b}{(V_G - V_C)/a} > \frac{1+\rho}{1-\rho} \approx 1.4, \qquad (3)$$

where V_A, V_G and V_C are the voltages of the anode, grid and cathode, respectively; a and b are the distances between the cathode and grid, and the grid and anode, respectively; $\rho = 2\pi r / d$, r is the radius of the grid wire and d is the space between grid wires. The value 1.4 was found for our chamber.

Fig. 6 shows that our result for a single grid chamber is in good agreement with condition (3). Gas mixture is the Ar+5%CO_2.

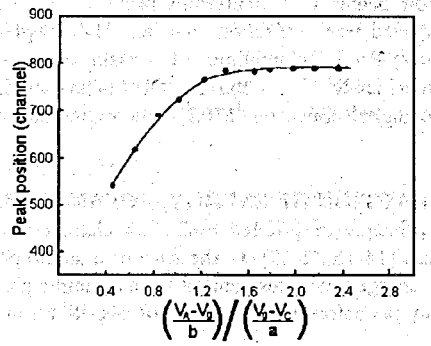

Fig. 6. Observed pulse height of the alpha source, indicating the fraction of electrons reaching the anode, versus the ratio of the field strength around the anode to that around the cathode

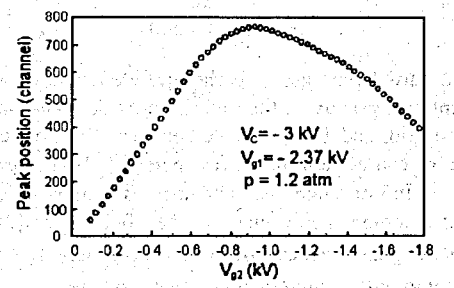

Fig. 7. The dependence of pulse height for the alpha source versus the second grid voltage at other fixed parameters

A similar procedure can be also made for the double grid chamber. Fig. 7 illustrates the dependence of the peak position for the alpha source on the voltage of the second grid at other fixed parameters. In this case the distances between electrodes are as follows: cathode - first grid = 3 cm, first and second grids = 5 cm, and second grid - anode = 2 cm. Fig. 7 shows that the optimum condition corresponds to $V_{g2} = -0.9$ kV. Then, values calculated by formula (3) for the ratios around the anode and around the cathode are 1.5 and 1.4, respectively, which are in agreement with condition (3).

It is also seen that for a double grid chamber the working condition, in comparison to a single grid one, is very sensitive to field strength ratios.

7.2. ENERGY CALIBRATION

The energy calibration, as mentioned above, was performed by means of a moving uranium or plutonium alpha source. Also, the capacity of our measurement system was tested using this alpha source. In Fig. 8. the three-dimensional energy spectrum of the anode and cathode signals is shown for the ^{238}Pu and ^{240}Pu alpha source for energies of 5.50 MeV and 5.17 MeV, respectively. From this spectrum the two-dimensional spectrum which is displayed in Fig. 9 can be obtained. Also from here, the energy spectra for the anode and cathode signals showed in Fig. 10 and Fig. 11, respectively can be obtained.

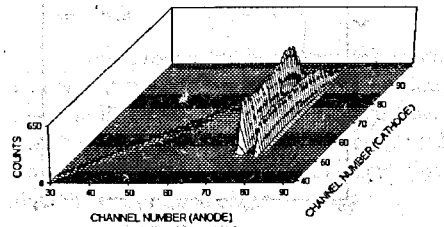

Fig. 8. The three - dimensional spectrum of the anode and cathode signals for the plutonium two peak alpha source

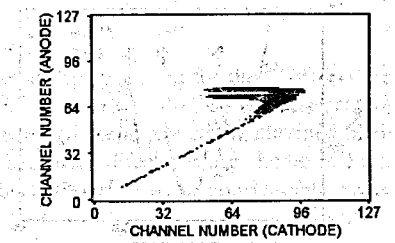

Fig. 9. The two-dimensional spectrum of the anode and cathode signals for the plutonium alpha-source

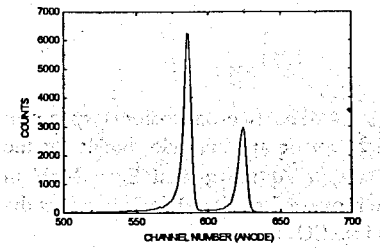

Fig. 10. Pulse height spectrum of the anode signal.

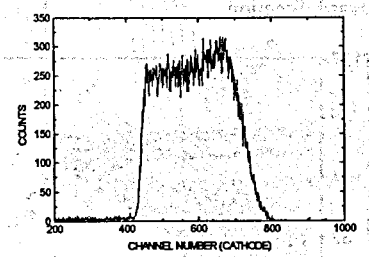

Fig. 11. Pulse height spectrum of the cathode signal.

7.3. ENERGY SPECTRA

The foreground and background energy spectra for the $^{64}Zn(n,\alpha)^{61}Ni$ reaction measured at E_n=5.1 MeV in the forward direction using the Ar+5%CO_2 gas mixture are shown in Figs. 12 and 13, respectively. The thickness of the isotope-sample was 0.72 mg/cm^2. The noticeable alpha peak from the $^{64}Zn(n,\alpha)^{61}Ni$ reaction can be seen. In addition to this peak, there are background peaks from the $^{36}Ar(n,\alpha)^{33}S$ reaction which considerably hamper experimental data handling. Nevertheless, we were able to measure the energy spectra, angular distribution and cross sections of the (n,α) reaction for ^{40}Ca and ^{64}Zn at E_n=4-5 MeV with a gas mixture of Ar+(3-5)%CO_2. The fact is that the two-dimensional spectra allows events of the sample placed on the cathode to be resolved from events of the working gas even though their energies are close. This feature is illustrated in Fig. 14 where the α_0 transition of the $^{40}Ca(n,\alpha)^{37}Ar$ reaction is located between the α_0 and α_1 transitions of the $^{36}Ar(n,\alpha)^{33}S$ reaction. The two-dimensional spectra clearly shows that the cathode signal of the α_0 for ^{40}Ca extends between channels of ~55 to ~90, at the time the cathode signals of the α_0 and α_1 for ^{36}Ar begin at nearly the 0 channel and reach to channels ~105 and ~96, respectively.

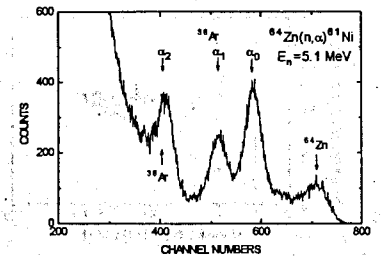

Fig. 12. The foreground energy spectrum of the $^{64}Zn(n,\alpha)^{61}Ni$ reaction measured with Ar+5%CO_2 at E_n=5.1 MeV in the forward direction.

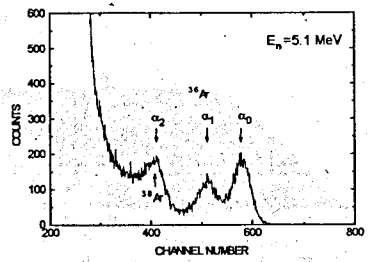

Fig. 13. The same as in Fig. 12 for background measurement.

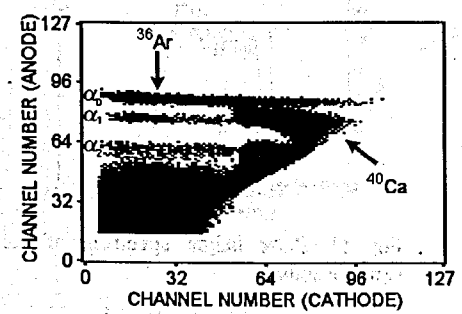

Fig. 14. The two-dimensional spectrum of the anode and cathode signals for the $^{40}Ca(n,\alpha)^{37}Ar$ reaction at E_n=5 MeV in the forward direction. Working gas is the Ar+5%CO_2 mixture.

In fig. 15 background subtracted energy spectra of the $^{40}Ca(n,\alpha)^{30}Ar$ reaction at E_n=5 MeV in the forward and backward directions are displayed. Alpha transitions to the excited states of ^{37}Ar can be seen, but the statistical accuracy and energy resolution for

these transitions are not high enough to calculate their intensities. In addition, the energy shift caused by reaction kinematics is seen.

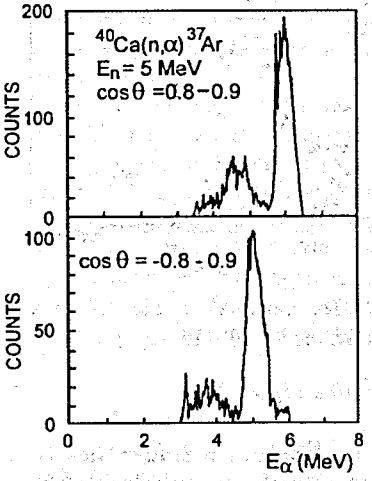

Fig. 15. Background subtracted energy spectra of the $^{40}Ca(n,\alpha)^{37}Ar$ reaction at E_n=5 MeV in the angular range of $cos\theta = 0.8 - 0.9$ (upper part) and $cos\theta = -0.8 - 0.9$ (lower part). Here θ is the angle between the direction of the incident beam and the direction of the emitted particle.

Foreground and background three-dimensional energy spectra for the $^{58}Ni(n,\alpha)^{55}Fe$ reaction at E_n=5.1 MeV in the forward direction using the Kr+1.7%CO_2 gas mixture are given in Figs. 16 and 17, respectively. Energy spectra of the anode signal obtained from the three-dimensional spectra in the forward and backward directions are shown in Figs. 18 and 19, respectively. It can be seen that the background of Kr is considerably lower than the background of Ar.

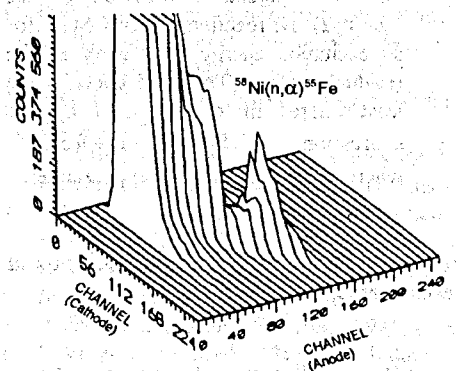

Fig. 16. The foreground three-dimensional energy spectrum of the anode and cathode signals for the $^{58}Ni(n,\alpha)^{55}Fe$ reaction in the forward (θ=0-75°) direction at E_n=5.1 MeV. Gas mixture is the Kr+1.7%CO_2.

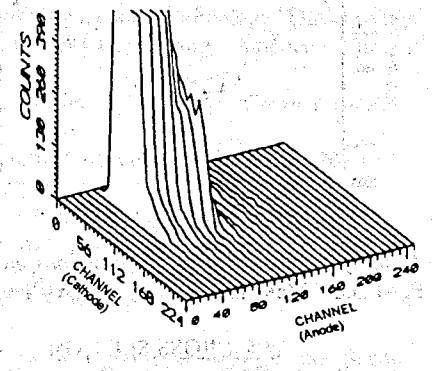

Fig. 17. The same as in Fig. 16 for background measurement.

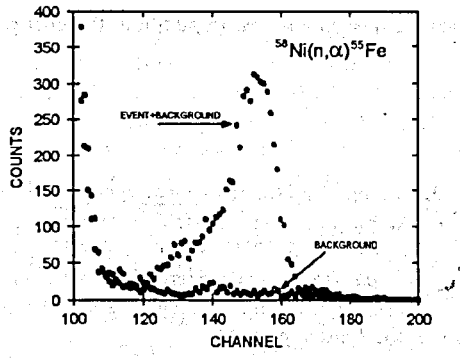

Fig. 18. Energy spectrum of the anode signal for the ^{58}Ni(n,α)^{55}Fe reaction in the forward direction (θ=0-75°) at E_n=5.1 meV.

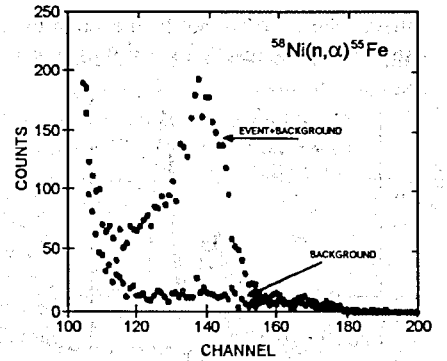

Fig. 19. The same as in Fig. 18 in the backward direction (θ=115-180°).

7.4. ANGULAR DISTRIBUTION

Our result for the angular distribution of the ^{64}Zn(n,α)^{61}Ni reaction at E_n=5 MeV is shown in the center-of-mass system in Fig. 20. Nearly symmetrical with respect to θ=90° the angular distribution is in agreement with the statistical model. But, this result is in disagreement with only other available forward peaked distributions, reported by Calvi et al. at E_n=4.5 and 5 MeV [27].

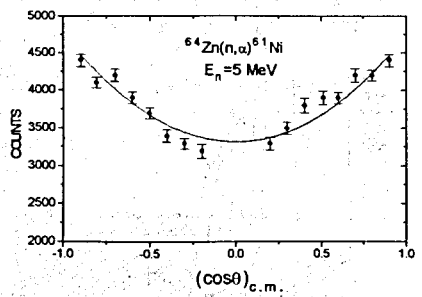

Fig. 20. Angular distribution of the ^{64}Zn(n,α)^{61}Ni reaction at E_n=5 MeV for an excitation energy E^*<2 MeV of the residual nucleus. The solid curve is the least-squares fit of our data by the expression $P(\cos\theta) = a + b\cos\theta^2$, where a and b are the fitting parameters.

Also, symmetrical angular distributions were observed for the ^{40}Ca(n,α)^{37}Ar reaction at E_n=4 and 5 MeV, and for the ^{58}Ni(n,α)^{55}Fe reaction at E_n=5 MeV [11,12].

7.5. CROSS SECTION

For the ^{40}Ca(n,α$_0$)^{37}Ar, ^{58}Ni(n,α)^{55}Fe and ^{64}Zn(n,α)^{61}Ni (for E^*<2 MeV) reactions using our experimental apparatuses and data acquisition and data processing system we obtained the angle integrated cross sections around E_n=5 MeV, which were found to be 234±23 mb, 47.4±5.0 mb and 34±3 mb, respectively [10-13].

CONCLUSION

1. Our experimental results have shown that the gridded twin ionization chamber can be successfully used to study the fast neutron induced charged particle emission reactions. It was found that krypton mixed with several percent dioxide carbon can be utilized for filling the ionization chamber as a low background working gas in the fast neutron beam.

2. The experimental techniques we used allow successful investigation of fast neutron induced (n,α) reactions for cross sections up to several mbarns to be carry out.

3. Our experimental data, as a whole, show that for the studied reactions, the compound nucleus mechanism predominates over other mechanisms. Nevertheless, to clarify the role of different reaction mechanisms it is necessary to perfect more detailed and exact measurements of the energy spectra, angular distributions and cross sections for the (n,α) reaction in the energy range of ~3 to ~10 MeV.

4. In the future, we are also planning to study the fast neutron induced (n,p) reactions for medium mass nuclei using our experimental method.

ACKNOWLEDGEMENT

The authors wish to thank P.V.Sedyshev, S.S.Parzhitskii and Yu.N.Voronov for their aid in the development of the ionization chambers, and the Van de Graaff accelerator crew for their help during the irradiation at the Institute of Heavy Ion Physics of Peking University.

The research described in this publication was made possible in part by Grant No RFI000 from the International Science Foundation and Grant No RFI300 from the ISF and Russian Goverment.

REFERENCES

1. D.C.Larson et al. In book: "Nuclear Data for Science and Technology" (Proceedings of the International Conference, May 9-13, 1994, Gatlinburg) American Nuclear Society, Inc. 1994, v.2, p.831.
2. E.Gadioli, P.E.Hodgson. Pre-Equilibrium Nuclear Reactions. Clarendon Press, Oxford, 1992.
3. V.M.Bychkov et al. Cross Sections for Threshold Reactions Produced by Neutrons. Energoatomizdat, Moscow, 1982 (in Russian).
4. V.McLane, C.L.Dunford, P.F.Rose. Neutron Cross Sections. Vol.2, Neutron Cross section Curves, BNL, Upton, New York, Academic Press, Inc. 1988.
5. K.R.Alvar et al. Nucl. Instr. Meth., 1978, v.148, N2, p.303.
6. M.Ahmad et al. Nucl. Instr. Meth., 1985, v.228A, N2/3, p.349.
7. A.Paulsen et al. Nucl. Sci. Eng., 1981, v.78, p.377.
8. H.Vonach. In book: "Neutron Induced Reactions" (Proceedings of the Second International Symposium, June 25-29, 1979, Smolenice). Ed. I.Ribanský and E.Běták, VEDA, Bratislava, 1980, p.59.
9. Yu.M.Gledenov et al. Annual Report 1990-1991. Laboratory of Neutron Physics, JINR, 92-59, p.121.
10. Tang Guoyou et al. Communication of Nuclear Data Progress. Chinese Nuclear Data Center, 1992, N8, Atomic Energy Press, Beijing, p.7.

11. Yu.M.Gledenov et al. In book: "Proceedings of the 8-th International Symposium on Capture Gamma-Ray Spectroscopy and Related Topics", Fribourg, Switzerland, 20-24 September, 1993. Ed. Jean Kern, World Scientific, Singapore, 1994, p.587.
12. Tang Guoyou et al. In book: "Neutron Spectroscopy, Nuclear Structure, Related Topics" (Proceedings of the Second International Seminar on Neutron-Nucleus Interactions, April 26-28, 1994, Dubna) JINR, E3-94-419, Dubna, 1994, p.253.
13. Yu.M.Gledenov et al. In abstract booklet: "Neutron Spectroscopy, Nuclear Structure, Related Topics" (III International Seminar on Interaction of Neutrons with Nuclei, April 26-28, 1995, Dubna) JINR, E3-95-119, Dubna,1995, p.28.
14. N.Ito, M.Baba et al. Nucl. Instr. Meth., 1994, v.337A, p.474.
15. A.Goverdovski et al. in ref.[1], p.117.
16. J.B.Marion, F.C.Yong. Nuclear Reaction Analysis. North-Holland. Publ. Co. Amsterdam, 1968.
17. J.Monahan. In book: "Fast Neutron Physics". Ed. J.B.Marion and J.L.Fowler. Part I. Interscience Publishers, New York, 1960.
18. Yu.P.Popov et al. Soviet J. of Nucl. Phys., 1980, v.32, p.459. Yadernaja Fizika, 1980, v.32, N4(10), p.893 (in Russian).
Yu.M.Gledenov et al. Prib. Techn. Eksp., 1988, p.55, N3, (in Russian).
19. R.R.Wilson. Rev. Sci. Instr., 1941, V.12, N2, p.91.
20. W.N.English, G.C.Hanna. Can. J. of Phys., 1953, v.31, N5, p.768.
21. Xia Songjiang. Chinese Journal of Nuclear Techniques. 1988, v.11, p.13.
22. Tang Guoyou et al. Chinese Journal of Nuclear Techniques. 1994, v.17, N3, p129.
23. C.Budtz-Jørgensen et al. Nucl. Instr. Meth., 1987, v.258A, N2, p.209.
24. O.Bunemann et al. Can. J. Res., 1949, v.27A, N5, p.191.
25. B.A.Bochagov et al. Izv. AN SSSR, ser. fiz. 1956, v.20, N12, p.1455.
26. A.A.Vorob'ev. In book: Techniques of measurements for radioactive samples. Ed. V.V.Bochkarev. Gosatomizdat, Moscow, 1962, p.18 (in Russian).
27. G.Calvi et al. In: Proc. Intern. Conf. on Nucl. Phys., 1964, Paris, v.2, p.724.